Laboratory of Pharmaceutical Proteomics[1], National Institute of Biomedical Innovation (NIBIO), Ibaraki; Graduate School of Pharmaceutical Sciences[2]; The Center of Advanced Medical Engineering and Informatics[3], Osaka University, Osaka, Japan

The specific effect of 2-methoxyestradiol on lymphatic vascular endothelial cells

S. Imai[1,2], Y. Yoshida[1,2], T. Okamura[1,2], K. Nagano[1,2], Y. Abe[1], T. Yoshikawa[1,2], H. Kamada[1,3], S. Nakagawa[2], S. Tsunoda[1,3], Y. Tsutsumi[1,2,3]

Received October 27, 2008, accepted November 28, 2008

Shin-ichi Tsunoda, Ph.D., Laboratory of Pharmaceutical Proteomics, National Institute of Biomedical Innovation, 7-6-8 Saito-Asagi, Ibaraki, Osaka 567-0085, Japan
tsunoda@nibio.go.jp

Pharmazie 64: 214–216 (2009) *doi: 10.1691/ph.2009.8776*

Lymphatic metastasis of tumors is one of the most important prognostic factors and provides valuable information for decisions on appropriate surgical protocols. Recent studies have demonstrated that lymphangiogenesis of lymphatic vascular endothelial cells into tumors is a key event in lymphatic metastasis. Therefore, control of lymphangiogenesis is a promising strategy for treatment or prevention of tumor metastasis and lymphatic disorders. However, mechanisms of lymphangiogenesis or its specific inhibition are not well-understood. In this study we examined effects of various types of signaling inhibitors on tube formation in human lymphatic microvascular endothelial cells (LECs) and blood microvascular endothelial cells (BECs) *in vitro*. We found that tube formation of LECs was specifically inhibited by 2-methoxyestradiol (2ME). This observation is of potential benefit in understanding the molecular mechanism of lymphangiogenesis. Furthermore, 2ME could therefore offer specific protection against lymphatic metastasis and lymphangiogenesis-related diseases.

1. Introduction

The major function of lymphatic vessels is to collect and transport interstitial fluid via lymph nodes, larger collecting lymphatic vessels and the thoracic duct, back to the blood circulation. The lymphatic system also contributes to the immune surveillance of the body by transporting activated immune cells from peripheral tissues to the regional lymph nodes. Recent reports indicate a contribution of the lymphatic system to various diseases, tumor metastasis, lymphedema, lymphangitis etc; (Alitalo et al. 2005; Stacker et al. 2002; Padera et al. 2002; Kerjaschki et al. 2004; Saban et al. 2004).

Tumor cells can take advantage of the lymphatic vascular system to promote their metastasis to lymph nodes and beyond. Indeed, tumor metastasis to regional (sentinel) lymph nodes often represents the first step in tumor dissemination and serves as a major prognostic indicator for the progression of human cancers. Recent studies have revealed that tumors can actively induce the formation of lymphatic vessels, and that tumor lymphangiogenesis promotes lymph node metastasis (Daiani et al. 2006; Hoshida et al. 2006; Harrell et al. 2007; Hirakawa et al. 2007). Recent evidence indicates that tumor cells can also induce lymph node lymphangiogenesis even before they metastasize, and that metastatic tumor cells continue to induce lymphatic vessel growth within sentinel lymph nodes, possibly promoting their further metastatic dissemination. Against this background, an approach involving inhibition of lymphangiogenesis in treating tumor metastasis is receiving considerable attention (He et al. 2002; Shimizu et al. 2004; He et al. 2005). One strategy has been to inhibit vascular endothelial growth factor receptor 3 (the receptor for one of the lymphangiogenesis signaling molecules). However, signaling via vascular endothelial growth factor receptor 3 is not lymphangiogenesis-specific. Because lymphatic vessel research is at an earlier stage compared with blood vessel research, lymphangiogenesis-specific molecules have not yet been

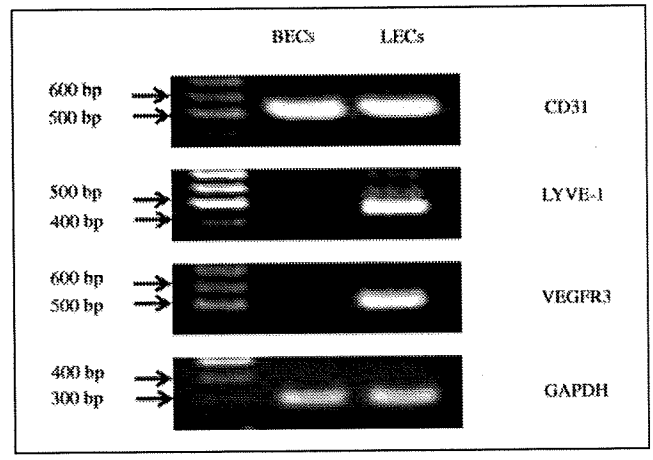

Fig. 1: Differential expression of vascular markers by BECs and LECs. RT-PCR analyses of CD31, LYVE-1, VEGFR-3 expression in BECs and LECs. RT-PCR analysis of D-glyceraldehyde-3-phosphate dehydrogenase (GAPDH) was performed as a loading control. Positions of base-pair markers are shown (bp).

identified, and very little marketing of lymphangiogenesis inhibitors has taken place.
Therefore, to identify inhibitors and study mechanisms of lymphangiogenesis, we examined effects of a diverse group of signaling inhibitors on tube formation in both lymphatic and blood vascular endothelial cells.

2. Investigations, results and discussion

We first characterized lymphatic and blood vessel endothelial phenotypes. This involved examination of gene expression profiles by RT-PCR in normal human lung lymphatic microvascular endothelial cells (LECs) and normal human lung blood microvascular endothelial cells (BECs) (Fig. 1). The pan-endothelial cell markers CD31/PECAM-1 were expressed in LECs and BECs. The lymphatic endothelial cell markers LYVE-1 and VEGFR-3/Flt-4 were restricted to LECs.

Secondly, we analyzed effects of diverse signaling inhibitors on LECs and BECs (Fig. 2). Inhibitors used were the known anti-cancer drugs D609 and 2ME. In both LECs and BECs treated with 2ME, no cellular cytotoxicity was observed over the range of inhibitor concentrations used. On the other hand, surprisingly, cell viability dose-dependently increased in both cell types treated with D609. Furthermore, the increase in LECs viability was greater than that of BECs. D609 is an inhibitor of phosphatidylcholine-specific phospholipase C or protein kinase C whose activation leads to proliferation of various cell types (tumor cells etc.) (Nofer et al. 2000; Catley et al. 2004). As a consequence, D609 is known as a general inhibitor of cell proliferation. However, our results conflict with this general view, indicating the possible presence of an unknown mechanism of action of D609. Moreover, we conclude from the greater increase observed in viability of LECs that the unknown mechanism may be mediated in an LEC-specific manner.

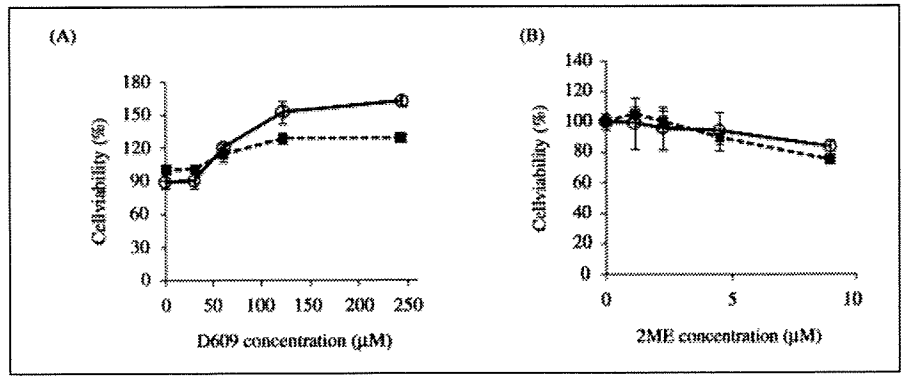

Fig. 2:
Effect of treatment with diverse inhibitors on cell viability of LECs and BECs. Effect of diverse inhibitors (D609, 2ME) on viability of LECs and BECs was assessed by MTT assay. After incubation of LECs/BECs in the absence or presence of inhibitors (D609, 2ME) for 24h, cell viability was measured with a microplate spectrophotometer at a wavelength of 450 nm.
(A) D609 (B) 2ME (circle; LECs), (filled box; BECs)

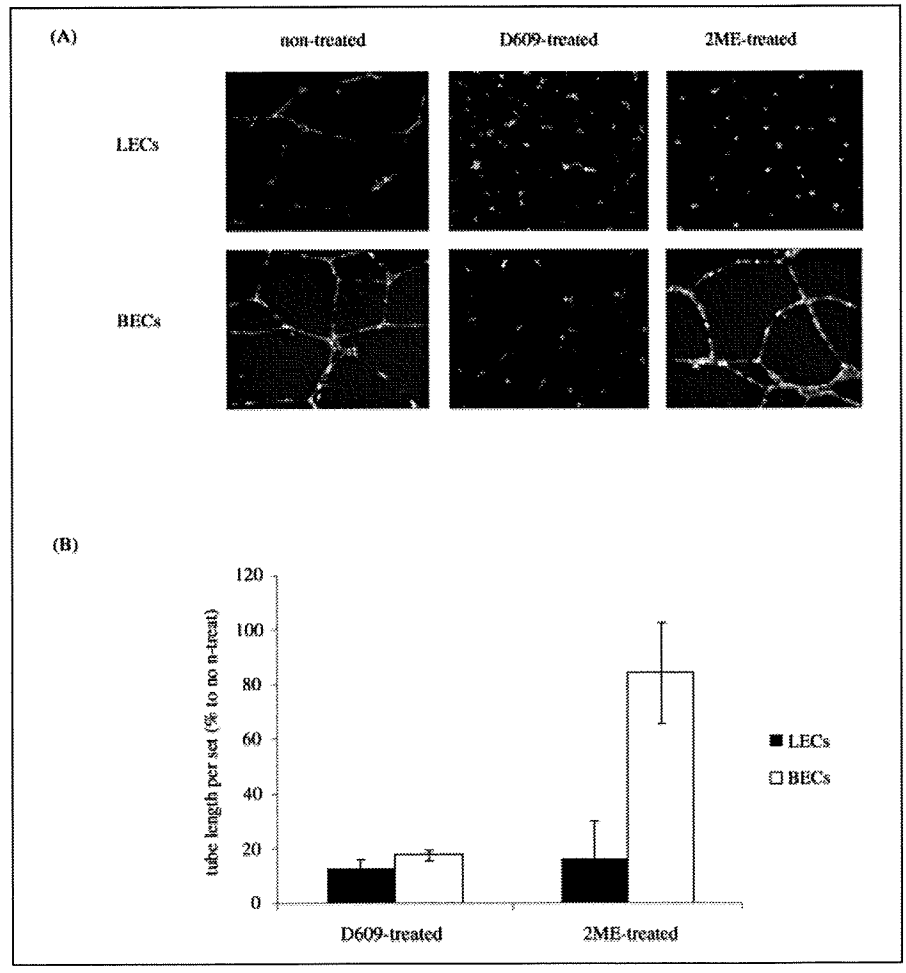

Fig. 3:
Effect of treatment with diverse inhibitors on tube formation by LECs and BECs. Effect of diverse inhibitors (D609, 2ME) on tube formation in LECs and BECs was assessed by tube formation assay. After incubation of LECs/BECs on Matrigel with inhibitors (D609, 2ME) for 24 h, tube formation in the two cell lines was observed using a microscope (A). (upper; LECs), (bottom; BECs) Total tube length for each condition was measured using MetaExpress (B). (filled column; LECs), (open column; BECs)

Finally, to identify inhibitors and study mechanisms of lymphangiogenesis, we analyzed effects of this diverse group of signaling inhibitors on tube formation in both LECs and BECs (Fig. 3). We found that D609 inhibited tube formation in both LECs and BECs. Meanwhile, 2ME inhibited tube formation specifically in LECs. From this result, we can conclude that 2ME may be a possible candidate drug for treatment of lymph node metastasis, which is related to lymphangiogenesis. 2ME is an inhibitor of hypoxia-inducible factor-1 (HIF-1) (Mooberry 2003; Becker et al. 2008; Zhou et al. 2008). HIF-1 is a master molecule which regulates expression of various cytokines (vascular endothelial growth factor, fibroblast growth factor etc.), and thereby a variety of cell biological responses such as tumor cell proliferation, angiogenesis etc. The present results demonstrating specific inhibition of tube formation in LECs may be because 2ME suppresses HIF-1 expression and activation of a lymphangiogenesis specific-factor. However, the detailed mechanism of this effect remains unknown. In the future, we expect that there will be many studies of lymphangiogenesis specific-signaling making use of the phenomenon described above.

In this report, we demonstrated that 2ME specifically inhibited lymphangiogenesis of LECs. Such a result increases the possibility of identifying candidate drugs for treatment of lymph node metastasis, which is related to lymphangiogenesis. Understanding the biology of LECs, including the identification of stimulators of lymphangiogenesis, represents another challenge for those researching tumor vascular biology. Finally, we believe that characterization of lymphangiogenesis-inhibitory drugs will provide important novel approaches for therapy of lymphangiogenesis-related diseases (tumor metastasis, lymphangitis etc.), along with new information on lymphatic vascular function in health and disease.

3. Experimental

3.1. Cell culture

Primary human lung-derived lymphatic microvascular endothelial cells (LECs),and blood microvascular endothelial cells (BECs) were purchased from Lonza (Basel, Switzerland), and maintained in culture medium, EGM-2-MV BulletKit (Lonza). These cells used for assays within 5 passages.

3.2. Reverse transcription and polymerase chain reaction

The mRNA expressions of endothelial markers on LECs and BECs were evaluated by semi-quantitative reverse transcription/polymerase chain reaction (RT-PCR). In brief, total RNA was extracted by using a TRIzol Reagent (Invitrogen) according to the manufacturer's protocols. First-strand cDNA was prepared from the RNA template (200 ng) using a random hexamer as a primer and SuperScript III reverse transcriptase (Invitrogen). The RT-reaction profile was 50 °C for 50 min, followed by 85 °C for 5 min. PCR amplification was performed by denaturation at 94 °C for 30 s, annealing at 60 °C or 55 °C for 1 min, and extension at 72 °C for 1 min and 1 min, by using template cDNA and KOD plus DNA polymerase (Toyobo). The sequences of the primers are listed as follows. CD31 sense; agcacagtggcaactacacg, CD31 antisense; gacgtcttcagtggggttgt, LYVE-1 sense; cacagggaaacacacctcct, LYVE-1 antisense; catcggcaacaatgaagaga, VEGFR3 sense; ctgctggaggaaaagtctgg, VEGFR3 antisense; gaggttgaccacgttgaggt, GAPDH sense; gtgaggtgaccgcatcttct, GAPDH antisense; tggaagatggtgatgggttt. The PCR products were electrophoresed in 1.5% agarose gels and detected by a CCD camera with ethidium bromide staining.

3.3. Cell viability assay

Viability of the cells after treatment with reagents was determined by a modified WST assay. Briefly, LECs and BECs were seeded at an initial density of 1×10^5 cells/ml in a 96-well plate for 24 h. Cells were then incubated with fresh medium containing various concentrations of diverse inhibitors for 24 h. The inhibitors used were D609 and 2-methoxyestradiol (2ME). All products were purchased from CALBIOCHEM. D609 concentrations were 0. 30.4, 60.8, 121.6, 243 (M; 2ME concentrations were 0. 1.12, 2.25, 4.5, 9 (M After incubation, WST was added to each well at a final concentration of 0.5 mg/ml. The insoluble formazan was collected, dissolved in dimethylsulfoxide (DMSO) and measured with a microplate spectrophotometer (Bio-Rad, U.S.A.) at a wavelength of 450 nm.

3.4. Tube formation assay

After coating with Matrigel (Becton, Dickinson and Company, Japan) in 24-well plates, LECs and BECs were seeded at a density of 6×10^5 cells/mL in each well and cultured overnight. Cells were then cultured for 5 h in basal medium only (control) or in basal medium containing diverse inhibitors (D609 243 μM, 2ME 9 μM). Tube formation area was observed using a microscope and was quantified by pixel counting. We calculated the mean value and SD using MetaExpress (Molecular Devices) according to the manufacturer's directions.

Acknowledgements: This study was supported in part by a Grant-in-Aid for Scientific Research (No.20015052 and 20790156) from the Ministry of Education, Culture, Sports, Science and Technology of Japan and in part by a Health and Labor Sciences Research Grant from the Ministry of Health, Labor and Welfare of Japan.

References

Alitalo K, Tammela T, Petrova TV (2005) Lymphangiogenesis in development and human disease. Nature 438: 946–953.

Becker CM, Rohwer N, Funakoshi T, Cramer T, Bernhardt W, Birsner A, Folkman J, D'Amato RJ (2008) 2-Methoxyestradiol inhibits hypoxia-inducible factor-1 {alpha} and suppresses growth of lesions in a mouse model of endometriosis. Am J Pathol 172: 534–544.

Catley MC, Cambridge LM, Nasuhara Y, Ito K, Chivers JE, Beaton A, Holden NS, Bergmann MW, Barnes PJ, Newton R (2004) Inhibition of protein kinase C (PKC) prevent activated transcription: role of events downstream of NF-kappaB DNA binding. J Biol Chem 279: 18457–18466

Daiani M, Kalchenko V, Yosepovich A, Margalit R, Hassid Y, Degani H, Seger D (2006) Real-time imaging of lymphogenic metastasis in orthotopic human breast cancer. Cancer Res 66 : 8037–8041.

He Y, Kozaki K, Karpanen T, Koshikawa K, Yla-Herttuala S, Takahashi T, Alitalo K (2002) Suppression of tumor lymphangiogenesis and lymph node metastasis by blocking vascular endothelial growth factor receptor 3 signaling. J National Cancer Inst 94: 819–825.

Harrell MI, Iritani BM, Ruddell A (2007) Tumor-induced sentinel lymph node lymphangiogenesis and increased lymph flow precede melanoma metastasis. Am J Pathol 170: 774–786.

He Y, Rajantie I, Pajusola K, Jeltsch M, Holopainen T, Yla-Herttuala S, Harding T, Jooss K, Takahashi T, Alitalo K (2005) Vascular endothelial cell growth factor receptor 3-mediated activation of lymphatic endothelium is crucial for tumor cell entry and spread via lymphatic vessels. Cancer Res 65: 4739–4746.

Hirakawa S, Brown LF, Kodama S, Paavonen K, Alitalo K, Detmar M (2007) VEGF-C-induced lymphangiogenesis in sentinel lymph nodes promoted tumor metastasis to distant sites. Blood 109: 1010–1017.

Hoshida T, Isaka N, Hagendoorn J, Tomaso ED, Chen Y, Pytowski B, Fukumura D, Padera TP, Jain RK (2006) Imaging steps of lymphatic metastasis reveals that vascular endothelial growth factor-C increases metastasis by increasing delivery of cancer cells to lymph nodes: therapeutic implications. Cancer Res 66: 8065–8075.

Kerjaschki D, Regele HM, Moosberger I, Nagy-Bojarski K, Watschinger B, Soleiman A, Birner P, Krieger S, Hovorka A, Silberhumer G, Laakkonen P, Petrova T, Langer B, Raab I (2004) Lymphatic neoangiogenesis in human kidney transplants is associated with immunologically active lymphocytic infiltrates. J Am Soc Nephrol 15: 603–612.

Mooberry SL (2003) Mechanism of action of 2-methoxyestradiol: new developments. Drug Resist Updat 6: 355–361.

Nofer JR, Junker R, Seedorf U, Assmann G, Zidek W and Tepel M (2000) D609-phosphatidylcholine-specific phospholipase C inhibitor attenuates thapsigargin-induced sodium influx in human lymphocytes. Cell Signal 12: 289–296.

Padera TP, Kadambi A, di Tomaso E, Carreira CM, Brown EB, Boucher Y, Choi NC, Mathisen D, Wain J, Mark EJ, Munn LL, Jain RK (2002) Lymphatic metastasis in the absence of functional intratumor lymphatics. Science 296: 1883–1886.

Saban MR, Mémet S, Jackson DG, Ash J, Roig AA, Israël A, Saban R (2004) Visualization of lymphatic vessels through NF-kappa B activity. Blood 104: 3228–3230.

Shimizu K, Kubo H, Yamaguchi K, Kawashima K, Ueda Y, Matsuo K, Awane M, Shimahara Y, Takabayashi A, Yamaoka Y, Satoh S (2004) Suppression of VEGFR-3 signaling inhibits lymph node metastasis in gastric cancer. Cancer Sci 95: 328–333.

Stacker SA, Achen MG, Jussila L, Baldwin ME, Alitalo K (2002) Lymphangiogenesis and cancer metastasis. Nature Rev Cancer 2: 573–583.

Zhou D, Matchett GA, Jadhav V, Dach N, Zhang JH (2008) The effect of 2-methoxyestradiol, a HIF-1 alpha inhibitor, in global cerebral ischemia in rats. Neurol Res 30: 268–271.

Acta Crystallographica Section F
Structural Biology and Crystallization Communications
ISSN 1744-3091
Editors: H. M. Einspahr and M. S. Weiss

Crystallization and preliminary X-ray analysis of the tumour necrosis factor α–tumour necrosis factor receptor type 2 complex

Yohei Mukai, Teruya Nakamura, Yasuo Yoshioka, Shin-ichi Tsunoda, Haruhiko Kamada, Shinsaku Nakagawa, Yuriko Yamagata and Yasuo Tsutsumi

Acta Cryst. (2009). F**65**, 295–298

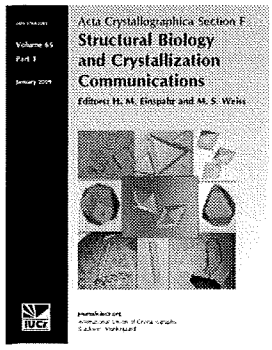

Acta Crystallographica Section F
Structural Biology and Crystallization Communications
ISSN 1744-3091

Crystallization and preliminary X-ray analysis of the tumour necrosis factor α–tumour necrosis factor receptor type 2 complex

Yohei Mukai,[a,b] Teruya Nakamura,[c] Yasuo Yoshioka,[b,d] Shin-ichi Tsunoda,[b] Haruhiko Kamada,[b] Shinsaku Nakagawa,[a] Yuriko Yamagata[c] and Yasuo Tsutsumi[a,b]*

[a]Graduate School of Pharmaceutical Sciences, Osaka University, Japan, [b]Laboratory of Pharmaceutical Proteomics, National Institute of Biomedical Innovation (NiBio), Japan, [c]Graduate School of Pharmaceutical Sciences, Kumamoto University, Japan, and [d]The Center of Advanced Medical Engineering and Informatics, Osaka University, Japan

Correspondence e-mail: ytsutsumi@phs.osaka-u.ac.jp

Received 29 September 2008
Accepted 7 February 2009

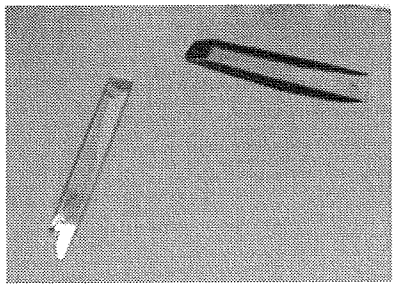

Tumour necrosis factor receptor type 2 (TNFR2, TNFRSF1B) is an essential receptor for various host-defence functions of tumour necrosis factor α (TNF). As part of studies to determine the structure of TNFR2, the formation, crystallization and preliminary X-ray diffraction analysis of the TNF–TNFR2 complex are described. The TNF–TNFR2 complex, which comprises one TNF trimer and three TNFR2 monomers, was confirmed and purified by size-exclusion chromatography. Crystals of the TNF–TNFR2 complex were obtained using polyethylene glycol 3350 as a precipitant. The crystal belonged to space group $P2_12_12_1$, with unit-cell parameters a = 74.5, b = 117.4, c = 246.8 Å. Assuming the presence of two TNF–TNFR2 complexes in the asymmetric unit, the Matthews coefficient V_M was 2.49 Å^3 Da^{-1} and the solvent content of the crystal was 50.7%. The crystal diffracted to 2.95 Å resolution.

1. Introduction

Tumour necrosis factor α (TNF) is a major inflammatory cytokine that plays a central role in host defence and inflammation (Aggarwal, 2003). Overexpression of TNF is closely associated with inflammatory diseases such as rheumatoid arthritis and inflammatory bowel disease (Feldmann & Maini, 2003). Therefore, anti-TNF antibodies and soluble TNF receptors (TNFR) that interfere with the activity of TNF have been used to treat various inflammatory diseases (Feldmann, 2002). However, anti-TNF therapy inhibits both types of TNFR (TNFR1 and TNFR2), often causing serious side effects.

Previous studies using animal models of diseases such as arthritis and hepatitis have demonstrated that TNFR1 plays a predominant role in the pathogenesis and exacerbation of inflammation (Mori *et al.*, 1996; Leist *et al.*, 1995). In contrast, TNFR2 is crucial for the proliferation, activation and antigen presentation of T cells, which are essential processes in the cell-mediated immune response against bacteria and viruses (Kafrouni *et al.*, 2003; Grell *et al.*, 1998). Therefore, blocking TNFR1-mediated signal transduction has emerged as a potential therapeutic strategy against inflammatory diseases with a low risk of side effects. Modelling the three-dimensional structure of the TNF–TNFR complex and understanding the differences between TNFR1 and TNFR2 will strongly contribute to the development of a TNFR1-selective therapeutic strategy.

To date, two crystal structures of TNFR1 have been reported: unliganded extracellular domains (PDB codes 1ncf and 1ext; Naismith *et al.*, 1995, 1996) and a lymphotoxin α (LT-α)–TNFR1 complex (PDB code 1tnr; Banner *et al.*, 1993). The structure of wild-type TNF has also been reported (PDB code 1tnf; Eck & Sprang, 1989). Several structures of TNF mutants, including the TNF mutant used in this experiment, have also been reported (PDB codes 1a8m, 2az5, 4tsv, 5tsw, 2e7a and 2zjc; Reed *et al.*, 1997; Cha *et al.*, 1998; Shibata *et al.*, 2008; Mukai *et al.*, 2009). However, the structure of TNFR2 has not yet been reported, although the structure of a viral protein with homology to TNFR2 has been solved (PDB code 2uwi; Graham *et al.*, 2007). This hinders the design of a structure-based drug for advanced anti-TNF therapy. Here, we describe the formation, crystallization and preliminary X-ray diffraction analysis of the

doi:10.1107/S1744309109004461

TNF–TNFR2 complex as part of our studies to determine the novel TNFR2 structure and aid in the development of TNFR1-selective therapies.

2. Methods

2.1. Preparation of TNF and TNFR2

The TNF molecule used in this experiment was a Lys-deficient TNF mutant [mutTNF Lys(−); K11M, K65S, K90P, K98R, K112N and K128P] created from wild-type TNF (wtTNF; NCBI accession No. X01394; Uniprot reference P01375) using a phage display system. This mutant retained full bioactivity and affinity for TNFR, as described previously (Yamamoto *et al.*, 2003). The wtTNF–TNFR2 complex formed efficiently, similar to that of mutTNF Lys(−) and TNFR2, but did not crystallize under the conditions described below.

MutTNF Lys(−) (residues 77–233 in Uniprot P01375; 157 amino acids, without tags) was expressed in *Escherichia coli* and refolded from inclusion bodies as described previously (Yamamoto *et al.*, 2003). Briefly, TNF was produced in *E. coli* BL21 (DE3) as inclusion bodies, which were washed in a buffer containing Triton X-100 and solubilized in 6 *M* guanidine–HCl, 0.1 *M* Tris–HCl pH 8.0 and 2 m*M* EDTA. Solubilized protein at 10 mg ml^{-1} was reduced with 65 m*M* dithioerythritol and refolded by a 100-fold dilution in a refolding buffer (100 m*M* Tris–HCl, 2 m*M* EDTA, 0.5 *M* arginine and 0.9 m*M* oxidized glutathione). After dialysis against 20 m*M* Tris–HCl pH 7.4 containing 100 m*M* urea, active trimeric proteins were purified by ion-exchange chromatography using Q-Sepharose FF (GE Healthcare Ltd). Size-exclusion chromatography was performed using a Superose 12 column (GE Healthcare) equilibrated with 20 m*M* Tris–HCl pH 7.4. The molecular mass of the purified TNF trimer was 51 kDa. The complete sequence of this TNF molecule was as follows: VRSSSRTPSD**M**PVAHVVANPQAEGQLQWLNRRANALLANG-VELRDNQLVVPSEGLYLIYSQVLF**S**GQGCPSTHVLLTHTISRI-AVSYQT**P**VNLLSAI**R**SPCQRETPEGAEA**N**PWYEPIYLGGVFQ-LE**P**GDRLSAEINRPDYLDFAESGQVYFGIIAL (residues mutated from wtTNF are shown in bold).

The extracellular domain of TNFR2 was used in this experiment (soluble TNFR2; NCBI accession No. M32315; Uniprot reference P20333). Purified soluble TNFR2 (residues 33–205 in Uniprot P20333; 173 amino acids, without tags) expressed in *E. coli* was purchased from PeproTech Inc. The molecular mass was 19 kDa as a monomer. The complete sequence of this TNFR2 molecule was as follows: APEPGSTCRLREYYDQTAQMCCSKCSPGQHAKVFC-TKTSDTVCDSCEDSTYTQLWNWVPECLSCGSRCSSDQVETQ-ACTREQNRICTCRPGWYCALSKQEGCRLCAPLRKCRPGFG-VARPGTETSDVVCKPCAPGTFSNTTSSTDICRPHQICNVVAIP-GNASMDAVCTSTSP. Lyophilized TNFR2 was dissolved in 20 m*M* Tris–HCl pH 7.4 and used directly for complex formation.

2.2. Purification of the TNF–TNFR2 complex

It is known that one TNF trimer binds three TNFR2 monomers and forms the TNF–TNFR2 complex. For crystallization of the complex, we attempted to purify the full 110 kDa TNF–TNFR2 complex (one 51 kDa TNF trimer and three 19 kDa soluble TNFR2 monomers). The complex was formed by mixing TNF and TNFR2 for 30 min at room temperature. Complex solutions with various molar ratios of TNF and TNFR2 were prepared and the molecular masses were assessed by analytical gel-filtration chromatography using a tandem Superdex 75 10/300 GL/Superdex 200 10/300 GL column (GE Healthcare) in 20 m*M* Tris–HCl pH 7.4 (Fig. 1). The use of two gel-filtration columns with different exclusion limits was useful for separating the complex from uncomplexed TNF and TNFR2. In this analysis, low-molecular-weight and high-molecular-weight gel-filtration calibration kits (GE Healthcare) were used as protein standards. An increase in the mixing ratio of TNFR2 induced a shift

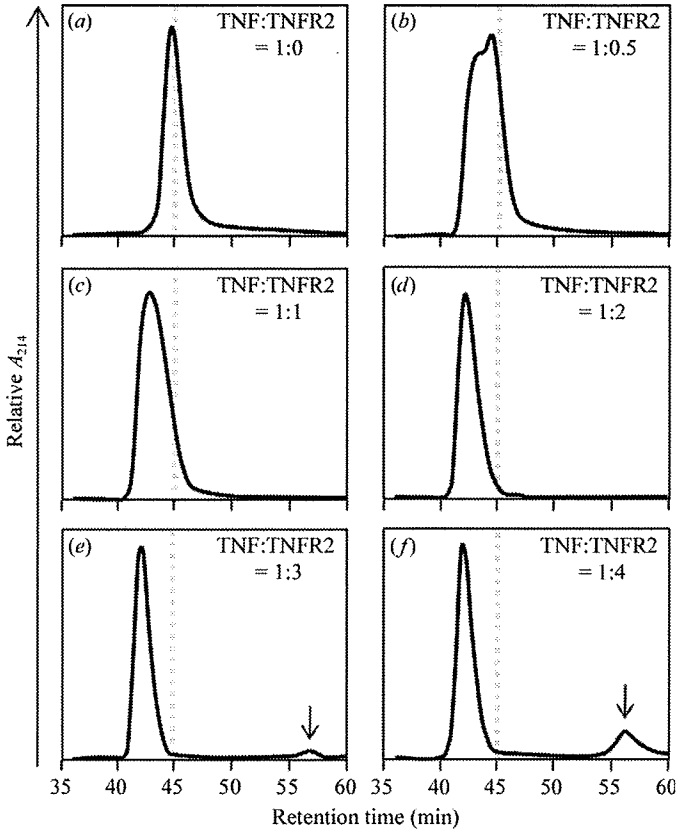

Figure 1
TNF–TNFR2 complex formation. Formation of the TNF–TNFR complex was assessed by analytical gel-filtration chromatography. The molar ratio of TNF trimer and TNFR2 was varied and the elution peak of the proteins was followed at 214 nm. The elution time of uncomplexed TNF occurs at 45 min (*a*). This is indicated by the broken grey line in (*a*)–(*f*). Excess unbound TNFR2 is indicated by arrows in (*e*) and (*f*).

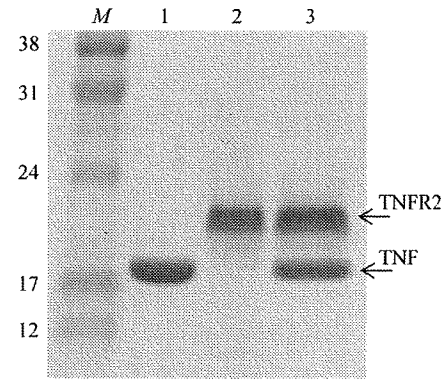

Figure 2
SDS–PAGE analysis of the TNF–TNFR2 complex. Formation of the TNF–TNFR2 complex was confirmed by SDS–PAGE. 15% polyacrylamide gel (ATTO Corp., Tokyo, Japan) was used to separate the bands containing TNF monomer (17 kDa) and TNFR2 monomer (19 kDa). *M*, Rainbow protein standard (labelled in kDa; GE Healthcare); lane 1, 2 µg TNF; lane 2, 2 µg TNFR2; lane 3, 4 µg purified TNF–TNFR2 complex.

in the retention peak of TNF to a higher molecular weight. At a TNF:TNFR2 ratio of 1:3 (Fig. 1*e*), a small peak at 57 min elution time corresponding to unbound 19 kDa TNFR2 was observed. This peak containing excess TNFR2 was also observed at a 1:4 ratio (Fig. 1*f*). This result indicated that the full 110 kDa TNF–TNFR2 complex was formed under these conditions. Therefore, final fractionation was performed between 41 and 44 min at a TNF:TNFR2 ratio of 1:4. The complex formation in the purified fraction was also confirmed by SDS–PAGE (Fig. 2). This full TNF–TNFR2 complex was concentrated to 10 mg ml^{-1} in 20 m*M* Tris–HCl pH 7.4 and used for crystallization as described below. The protein concentration was determined using Coomassie Protein Assay Reagent (Thermo Fisher Scientific Inc.).

2.3. Crystallization of the TNF–TNFR2 complex

The sparse-matrix screening kit Crystal Screen HT and the systematic salt and PEG screening kit Index HT (Hampton Research, Aliso Viejo, California, USA) were used for initial crystallization trials using the sitting-drop vapour-diffusion method. Drops consisting of 0.5 µl protein solution (10 mg ml^{-1}) and 0.5 µl reservoir solution were equilibrated against 100 µl reservoir solution in a Crystal*EX* 96-well flat-bottom plate (Corning Incorporated, Corning, New York, USA). Two temperatures, 293 and 277 K, were tested. Microcrystals were obtained using reservoir solution containing 20%(*w*/*v*) PEG 3350 and 0.2 *M* sodium formate at 293 K. A grid screen around these conditions was evaluated using the hanging-drop vapour-diffusion method. In this step, a drop consisting of 1 µl protein solution and 1 µl reservoir solution was equilibrated against 250 µl reservoir solution in a 24-well VDX Plate (Hampton Research). The crystallization conditions were improved using an additive screening kit (Hampton Research) and round-edged plate-shaped crystals were obtained from a droplet consisting of 1 µl 5 mg ml^{-1} protein solution and 1 µl reservoir solution containing 8%(*w*/*v*) PEG 3350, 0.2 *M* sodium formate and 0.02 *M* cobalt(II) chloride as an additive reagent. Protein and additive concentrations were optimized and the best crystals were obtained using 7.5 µl 0.8 mg ml^{-1} protein solution and 7.5 µl reservoir solution containing 7.5%(*w*/*v*) PEG 3350, 0.2 *M* sodium formate and 0.06 *M* cobalt(II) chloride. The crystals used for data collection had typical dimensions of 0.2 × 0.1 × 0.03 mm (Fig. 3).

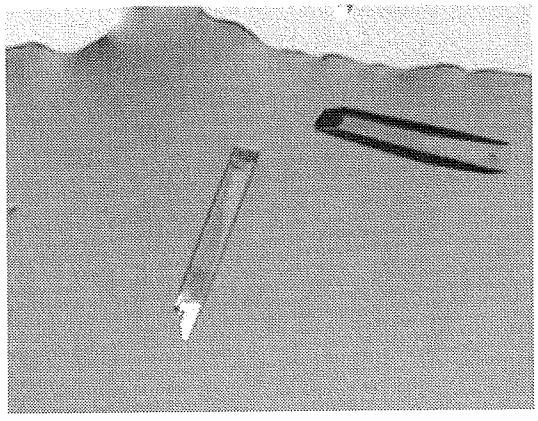

Figure 3
TNF–TNFR2 crystals. Two crystals of the TNF–TNFR2 complex with approximate dimensions of 0.2 × 0.1 × 0.03 mm are shown.

Table 1
Data-collection statistics for the TNF–TNFR2 complex.

Values in parentheses are for the highest resolution shell.

X-ray source	SPring-8 BL41XU
Wavelength (Å)	1.000
Space group	$P2_12_12_1$
Unit-cell parameters	a = 74.5, b = 117.4, c = 246.8
Resolution range (Å)	50–2.95 (3.06–2.95)
Observed reflections	744297
Unique reflections	45945 (4075)
Completeness (%)	98.9 (89.8)
$R_{\rm merge}$† (%)	0.183 (0.603)
$\langle I/\sigma(I)\rangle$	10.75 (1.51)

† $R_{\rm merge} = \sum_{hkl}\sum_i |I_i(hkl) - \langle I(hkl)\rangle| / \sum_{hkl}\sum_i I_i(hkl)$, where $I_i(hkl)$ is the ith intensity measurement of reflection hkl, including symmetry-related reflections, and $\langle I(hkl)\rangle$ is its average.

2.4. Preliminary X-ray analysis

X-ray diffraction experiments were performed on BL41XU of the SPring-8 Synchrotron Facility in Harima, Japan. An ADSC Quantum 315 X-ray CCD detector was installed on BL41XU and used to record the diffraction data. Crystals were soaked in a cryoprotectant solution composed of 7.5%(*w*/*v*) PEG 3350, 0.2 *M* sodium formate, 0.06 *M* cobalt(II) chloride and 30% glycerol. The crystals were then mounted in nylon loops (Hampton Research) and flash-cooled in a nitrogen stream at 95 K. Diffraction data were collected in 1.0° oscillation steps (180 images, 0–180°) and the crystal diffracted X-rays to 2.95 Å resolution. The data set was processed and scaled using the *HKL*-2000 program (Otwinowski & Minor, 1997). The crystals belonged to space group $P2_12_12_1$, with unit-cell parameters a = 74.5, b = 117.4, c = 246.8 Å. Data-collection statistics are shown in Table 1.

3. Results and discussion

The results of SDS–PAGE using the crystallization solution suggested that the crystal contained both TNF and TNFR2. Gel-filtration analysis showed that the TNF–TNFR2 complex with a molecular mass of 110 kDa contained both a TNF trimer (51 kDa) and three TNFR2 monomers (3 × 19 kDa). This suggests that the asymmetric unit of the crystals contained two molecules of the TNF–TNFR2 complex (two TNF trimers and six TNFR2 monomers). The calculated solvent content was 50.7% and the Matthews coefficient was 2.49 Å^3 Da^{-1} (Matthews, 1968).

Molecular replacement was performed with the *MOLREP* program (Vagin & Teplyakov, 1997) in *CCP4i* (Potterton *et al.*, 2003) using the TNF mutant structure described in our previous report (PDB code 2e7a; Shibata *et al.*, 2008) as a search model. Two significant solutions corresponding to TNF trimers were obtained (R = 0.469). The model from molecular replacement was subjected to rigid-body refinement, simulated annealing, energy minimization and B-factor refinement using *CNS* (Brünger *et al.*, 1998). The initial electron-density map calculated using only the phases of refined TNF trimer structures (R = 0.425 and $R_{\rm free}$ = 0.493) clearly showed almost the entire TNF trimer. The main chains and side chains of TNFR2 could also be detected around the TNF trimer. Manual model building of TNFR2 based on the TNFR1 structure using the *Coot* program (Emsley & Cowtan, 2004) in *CCP4i* is in progress.

This study was supported by Research for Promoting Technological Seeds (No. 11-067) from the Japan Science and Technology Agency (JST), Research Fund Project on Health Sciences focusing on Drug Innovation (No. KAA3701) from the Japan Health Sciences

Foundation, grants from the Ministry of Health, Labor and Welfare in Japan, a Grant-in-Aid for Young Scientists (B) (No. 20790134) and Grants-in-Aid for Scientific Research (Nos. 17016084, 17689008, 17790135, 18015055, 18659047, 20015052 and 20200017) from the Ministry of Education, Culture, Sports, Science and Technology of Japan (MEXT) and Research Fellowships for Young Scientists (No. 20-3919) from Japan Society for the Promotion of Science (JSPS). This study was also supported by Hayashibara Biochemical Laboratories Inc., Okayama, Japan.

References

Aggarwal, B. B. (2003). *Nature Rev. Immunol.* **3**, 745–756.
Banner, D. W., D'Arcy, A., Janes, W., Gentz, R., Schoenfeld, H. J., Broger, C., Loetscher, H. & Lesslauer, W. (1993). *Cell*, **73**, 431–445.
Brünger, A. T., Adams, P. D., Clore, G. M., DeLano, W. L., Gros, P., Grosse-Kunstleve, R. W., Jiang, J.-S., Kuszewski, J., Nilges, M., Pannu, N. S., Read, R. J., Rice, L. M., Simonson, T. & Warren, G. L. (1998). *Acta Cryst.* D**54**, 905–921.
Cha, S. S., Kim, J. S., Cho, H. S., Shin, N. K., Jeong, W., Shin, H. C., Kim, Y. J., Hahn, J. H. & Oh, B.-H. (1998). *J. Biol. Chem.* **273**, 21253–21260.
Eck, M. J. & Sprang, S. R. (1989). *J. Biol. Chem.* **264**, 17595–17605.
Emsley, P. & Cowtan, K. (2004). *Acta Cryst.* D**60**, 2126–2132.
Feldmann, M. (2002). *Nature Rev. Immunol.*, **2**, 364–371.
Feldmann, M. & Maini, R. N. (2003). *Nature Med.* **9**, 1245–1250.
Graham, S. C., Bahar, M. W., Abrescia, N. G., Smith, G. L., Stuart, D. I. & Grimes, J. M. (2007). *J. Mol. Biol.* **372**, 660–671.
Grell, M., Becke, F. M., Wajant, H., Mannel, D. N. & Scheurich, P. (1998). *Eur. J. Immunol.* **28**, 257–263.
Kafrouni, M. I., Brown, G. R. & Thiele, D. L. (2003). *J. Leukoc. Biol.* **74**, 564–571.
Leist, M., Gantner, F., Jilg, S. & Wendel, A. (1995). *J. Immunol.* **154**, 1307–1316.
Matthews, B. W. (1968). *J. Mol. Biol.* **33**, 491–497.
Mori, L., Iselin, S., De Libero, G. & Lesslauer, W. (1996). *J. Immunol.* **157**, 3178–3182.
Mukai, Y., Shibata, H., Nakamura, T., Yoshioka, Y., Abe, Y., Nomura, T., Taniai, M., Ohta, T., Ikemizu, S., Nakagawa, S., Tsunoda, S., Kamada, H., Yamagata, Y. & Tsutsumi, Y. (2009). *J. Mol. Biol.* **30**, 1121–1129.
Naismith, J. H., Devine, T. Q., Brandhuber, B. J. & Sprang, S. R. (1995). *J. Biol. Chem.* **270**, 13303–13307.
Naismith, J. H., Devine, T. Q., Kohno, T. & Sprang, S. R. (1996). *Structure*, **4**, 1251–1262.
Otwinowski, Z. & Minor, W. (1997). *Methods Enzymol.* **276**, 307–326.
Potterton, E., Briggs, P., Turkenburg, M. & Dodson, E. (2003). *Acta Cryst.* D**59**, 1131–1137.
Reed, C., Fu, Z. Q., Wu, J., Xue, Y. N., Harrison, R. W., Chen, M. J. & Weber, I. T. (1997). *Protein Eng.* **10**, 1101–1107.
Shibata, H. *et al.* (2008). *J. Biol. Chem.* **283**, 998–1007.
Vagin, A. & Teplyakov, A. (1997). *J. Appl. Cryst.* **30**, 1022–1025.
Yamamoto, Y., Tsutsumi, Y., Yoshioka, Y., Nishibata, T., Kobayashi, K., Okamoto, T., Mukai, Y., Shimizu, T., Nakagawa, S., Nagata, S. & Mayumi, T. (2003). *Nature Biotechnol.* **21**, 546–552.

doi:10.1016/j.jmb.2008.11.053 J. Mol. Biol. (2009) 385, 1221–1229

JMB

Available online at www.sciencedirect.com

ScienceDirect

ELSEVIER

Structure–Function Relationship of Tumor Necrosis Factor (TNF) and Its Receptor Interaction Based on 3D Structural Analysis of a Fully Active TNFR1-Selective TNF Mutant

Yohei Mukai[1,2], Hiroko Shibata[2], Teruya Nakamura[3], Yasuo Yoshioka[2,4], Yasuhiro Abe[2], Tetsuya Nomura[1,2], Madoka Taniai[5], Tsunetaka Ohta[5], Shinji Ikemizu[3], Shinsaku Nakagawa[1], Shin-ichi Tsunoda[2], Haruhiko Kamada[2], Yuriko Yamagata[3] and Yasuo Tsutsumi[1,2*]

[1]*Graduate School of Pharmaceutical Sciences, Osaka University, 1-6 Yamadaoka, Suita, Osaka 565-0871, Japan*

[2]*Laboratory of Pharmaceutical Proteomics, National Institute of Biomedical Innovation, Osaka 567-0085, Japan*

[3]*Graduate School of Pharmaceutical Sciences, Kumamoto University, Kumamoto 862-0973, Japan*

[4]*The Center for Advanced Research and Education in Drug Discovery and Development, Osaka University, 1-6 Yamadaoka, Suita, Osaka 565-0871, Japan*

[5]*Hayashibara Biochemical Laboratories, Inc., 1-2-3 Shimoishii, Okayama 702-8006, Japan*

Received 9 July 2008; received in revised form 21 November 2008; accepted 22 November 2008
Available online 6 December 2008

Edited by I. Wilson

Tumor necrosis factor (TNF) is an important cytokine that suppresses carcinogenesis and excludes infectious pathogens to maintain homeostasis. TNF activates its two receptors [TNF receptor (TNFR) 1 and TNFR2], but the contribution of each receptor to various host defense functions and immunologic surveillance is not yet clear. Here, we used phage display techniques to generate receptor-selective TNF mutants that activate only one TNFR. These TNF mutants will be useful in the functional analysis of TNFR.

Six amino acids in the receptor binding interface (near TNF residues 30, 80, and 140) were randomly mutated by polymerase chain reaction. Two phage libraries comprising over 5 million TNF mutants were constructed. By selecting the mutants without affinity for TNFR1 or TNFR2, we successfully isolated 4 TNFR2-selective candidates and 16 TNFR1-selective candidates, respectively. The TNFR1-selective candidates were highly mutated near residue 30, whereas TNFR2-selective candidates were highly mutated near residue 140, although both had conserved sequences near residues 140 and 30, respectively. This finding suggested that the phage display technique was suitable for identifying important regions for the TNF interaction with TNFR1 and TNFR2. Purified clone R1-6, a TNFR1-selective candidate, remained fully bioactive and had full affinity for TNFR1 without activating TNFR2, indicating the usefulness of the R1-6 TNF mutant in analyzing TNFR1 receptor function.

To further elucidate the receptor selectivity of R1-6, we examined the structure of R1-6 by X-ray crystallography. The results suggested that R31A and R32G mutations strongly influenced electrostatic interaction with TNFR2, and that L29K mutation contributed to the binding of R1-6 to TNFR1. This phage display technique can be used to efficiently construct functional mutants for analysis of the TNF structure–function relationship, which might facilitate *in silico* drug design based on receptor selectivity.

Keywords: TNF; X-ray crystallography; phage display system; TNF mutant; receptor specificity

*Corresponding author. Department of Toxicology, Graduate School of Pharmaceutical Sciences, Osaka University, 1-6 Yamadaoka, Suita, Osaka 565-0871, Japan. E-mail address: ytsutsumi@phs.osaka-u.ac.jp.

Abbreviations used: TNF, tumor necrosis factor; TNFR, TNF receptor; SPR, surface plasmon resonance; wtTNF, wild-type TNF; PDB, Protein Data Bank.

Introduction

Tumor necrosis factor (TNF) is as an important immunity-modulating cytokine that is required for human body defense against infectious diseases and carcinogenesis.[1] Excess TNF, however, causes various autoimmune diseases, such as rheumatoid arthritis, Crohn's disease, and ulcerative colitis.[2–4] The relationship between TNF and disease deterioration must be unraveled before effective therapies can be developed. Both TNF receptor (TNFR) types TNFR1 and TNFR2, which induce different cell signaling, must be analyzed to better understand the function of TNF. Experiments with TNFR knockout mice have revealed the individual functions of TNFR1 and TNFR2 against viral infection, microbial pathogens, and tumor immunity.[5–8] The lack of one TNFR type, however, can affect the function of the other receptor type and weaken its signaling because the two receptors work together by crosstalk signaling.[9–11] This issue complicates investigations of the individual roles of TNFR1 and TNFR2, and the analysis of TNFR function. Therefore, many researchers have attempted to activate only one receptor using a receptor-selective TNF mutant that does not impair the function of the receptor.

In the past decade, several receptor-selective TNF mutants, which are useful for functional analysis of TNFRs, have been constructed.[12,13] Traditional point mutation methods, however, are labor-intensive because a large number of candidates must be individually assessed; therefore, it has been difficult to successfully isolate the desired mutants.[14–17] In particular, a receptor-selective TNF mutant with full bioactivity was difficult to develop due to the fact that a region on TNF shares a binding affinity for the two different receptors.[18,19] Furthermore, inadequate mutations cause a loss of affinity for both TNFR1 and TNFR2, which has made it difficult to create novel mutants with high selectivity and full bioactivity.[20] Therefore, functional analysis of TNFR using these mutants has not progressed sufficiently.

We previously developed a modified phage display technique that can be used to create desired functional mutant proteins. Using this technique, we have successfully created many mutants with high bioactivity,[21] high *in vivo* stability,[22] and antagonist activity[23] that are suitable for drug development. The advantage of this method is that it allows us to obtain information about specific functions and associated sequences, which is very useful for determining the structure–function relationship of a specific protein. This information will be useful for improving the design of therapeutic mutants.

In the present study, we used the phage display technique to create novel receptor-selective TNF mutants with full bioactivity. Structural information of the mutants was determined by crystallographic analysis, and structural simulation was used to determine a feasible basis for receptor selectivity. These TNF mutants will be useful tools for analyzing TNFR signaling. An understanding of the structure and sequence of these functional mutants, combined with bioinformatics techniques, can potentially lead to the design of a desired functional protein, peptide, or peptide mimic, and thus accelerate the development of novel strategies for analyzing disease-related proteins, such as TNF, and the development of associated therapies.

Results

Library construction and selection of receptor-selective TNF mutants

To create receptor-specific TNF mutants using our phage display system, we prepared two phage libraries, Libraries I and II. Each library contained six amino acids randomized in a receptor binding site suggested by point mutation analysis and X-ray crystallography (Fig. 1).[16,17,24] For construction of the TNF mutant library, a mutant TNF-Lys(−) gene was used as template for polymerase chain reaction (PCR) mutagenesis.[22] Sequence analysis of randomly selected clones indicated that Libraries I and II contained 8.2×10^6 and 5.6×10^6 independent clones, respectively. For selection from the library, several rounds of affinity panning were performed against human TNFR1 or TNFR2 using BIAcore 3000. Potent binders to TNFR1 or TNFR2 were concentrated in the library through this panning procedure. The monoclonal candidates in each library were picked up for enzyme-linked immunosorbent assay (ELISA) screening to confirm their receptor binding specifi-

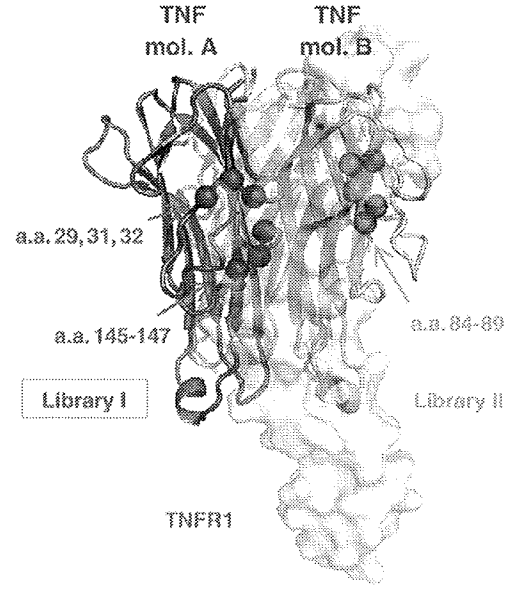

Fig. 1. Positions of randomized residues on the binding interface of the TNF–TNFR1 complex. Mutational residues of Library I (red spheres) and Library II (orange spheres). Green cartoon represents wtTNF. White area represents the surface of the TNFR1 monomer. This binding model structure of the TNF–TNFR1 complex was constructed based on the crystal structure of the LTα–TNFR1 complex (1TNR) and that of wtTNF (1TNF).

Table 1. Substituted residues of TNF mutants from Libraries I and II

			29	31	32	84	85	86	87	88	89	145	146	147
		wtTNF	L	R	R	A	V	S	Y	Q	T	A	E	S
		mutTNF-Lys(−)	—	—	—	—	—	—	—	—	—	—	—	—
TNFR1-selective candidates	Library I (29:32–145:147)	R1-1	I	—	—	—	—	—	—	—	—	—	—	—
		R1-2	Q	—	W	—	—	—	—	—	—	—	—	—
		R1-3	T	G	Y	—	—	—	—	—	—	—	—	—
		R1-4	T	K	Y	—	—	—	—	—	—	—	—	—
		R1-5	T	—	F	—	—	—	—	—	—	—	T	—
		R1-6	K	A	G	—	—	—	—	—	—	—	S	T
	Library II (84:89)	R1-7	—	—	—	S	K	T	—	T	H	—	—	—
		R1-8	—	—	—	S	P	L	—	P	K	—	—	—
		R1-9	—	—	—	S	T	N	—	N	G	—	—	—
		R1-10	—	—	—	T	S	A	—	G	P	—	—	—
		R1-11	—	—	—	T	T	A	—	S	G	—	—	—
		R1-12	—	—	—	T	H	K	—	P	Q	—	—	—
		R1-13	—	—	—	S	K	T	—	S	H	—	—	—
		R1-14	—	—	—	S	S	H	—	R	F	—	—	—
TNFR2-selective candidates	Library I (29:32–145:147)	R2-1	—	—	—	—	—	—	—	—	—	K	D	T
		R2-2	—	—	—	—	—	—	—	—	—	R	T	D
		R2-3	—	—	—	—	—	—	—	—	—	R	E	T
		R2-4	—	—	—	—	—	—	—	—	—	A	D	D
		R2-5	—	—	—	—	—	—	—	—	—	A	N	D

Conserved residues compared with wtTNF are indicated by an em dash (—). Mutated residues in each library are highlighted in gray. Library I included mutated residues 29, 31, 32, and 145–147. Library II contained mutated residues 84–89. R1-1–R1-6 and R1-7–R1-14 were isolated from Libraries I and II, respectively, as TNFR1-selective candidates. TNFR2-selective clones R2-1–R2-5 were isolated from Library I; Library II contained no TNFR2-selective clones.

city. Several clones with TNFR1 or TNFR2 specificity were eventually obtained.

Sequence analysis of receptor-specific TNF mutant candidates

Sequence analysis revealed that we had 14 TNFR1-selective candidates (R1-1–R1-14) and 5 TNFR2-selective candidates (R2-1–R2-5) from Libraries I and II (Table 1). Unfortunately, Library II did not contain any TNFR2-selective mutants. All active TNFR1-selective mutants in Library II retained Tyr87, suggesting that Tyr87 was an essential residue for receptor binding. Analysis of Library I, however, revealed that the mutated and conserved regions of the TNFR1-selective mutants were different from

Table 2. Receptor-selective bioactivities and affinities of TNF mutants

			Relative affinity (% K_d)[a]			Relative bioactivity (% of EC_{50})		
		TNFs	TNFR1	TNFR2	R_1/R_2	HEp2[b]	PC60[c]	R_1/R_2
		wtTNF	100	100	1.0	100	100	1.0
		mutTNF-Lys(−)	108	88	1.2	116	126	0.9
TNFR1-selective candidates	Library I (29:32–145:147)	R1-1	145	121	1.2	492	NT	—
		R1-2	212	32	6.7	436	NT	—
		R1-3	42	18	2.4	343	NT	—
		R1-4	43	3	13.4	447	NT	—
		R1-5	177	2	106.2	582	36	16.2
		R1-6	33	4	8.4	128	<0.07	>1800.0
	Library II (84:89)	R1-7	108	13	8.4	102	NT	—
		R1-8	145	9	16.5	120	173	0.7
		R1-9	175	24	7.4	110	NT	—
		R1-10	149	9	17.0	134	NT	—
		R1-11	219	11	20.4	58	NT	—
		R1-12	51	15	3.5	21	NT	—
		R1-13	51	11	4.6	26	NT	—
		R1-14	46	4	12.0	47	47	1.0
TNFR2-selective candidates	Library I (29:32–145:147)	R2-1	83	112	0.741	12.4	23	0.539
		R2-2	3	143	0.020	0.2	30	0.007
		R2-3	38	225	0.169	2.5	12	0.208
		R2-4	51	572	0.089	6.2	19	0.326
		R2-5	94	324	0.290	13.4	39	0.344

The affinity and bioactivity values are shown as relative values (% wtTNF).

NT, not tested.

[a] Affinity for immobilized TNFR1 and TNFR2 was assessed by SPR using BIAcore 3000.

[b] Human TNFR1-mediated bioactivity was evaluated using a HEp-2 cell cytotoxicity assay. In this assay, HEp-2 cell viability was determined by methylene blue staining. Each value represents the mean±SD.

[c] Human TNFR2-mediated bioactivity was evaluated using PC60-R2 assay. GM-CSF expression by TNFR2-mediated signaling was detected by ELISA. Each value presents the mean±SD.

those of the TNFR2-selective mutants. TNFR1-selective mutants were highly mutated near residue 30 and conserved near residue 140. On the other hand, TNFR2-selective mutants were mutated near residue 140 and conserved near residue 30. This interesting result suggested that the details of the essential binding interface for TNFR1 and TNFR2 differed despite their predicted similar complex forms.[19]

Receptor selectivity and bioactivity of TNF mutants

To investigate the properties of candidate receptor-selective TNF mutants in detail, we prepared recombinant protein using the previously described methods.[21,22] TNF mutants expressed as an inclusion body in *Escherichia coli* were denatured and refolded. Then, active TNF mutants were purified by ion-exchange and gel-filtration chromatography. TNF mutant purity was greater than 90% in sodium dodecyl sulfate–polyacrylamide gel electrophoresis, and all mutants were confirmed to form trimers by gel-filtration analysis (data not shown).

We examined the affinities of these recombinant TNF mutants for TNFR1 and TNFR2 (Table 2). Most of the TNFR1-selective candidates had little affinity for TNFR2 based on surface plasmon resonance (SPR) analysis by BIAcore 3000. In particular, the TNFR1 affinities of R1-2, R1-5, R1-8, R1-9, R1-10, and R1-11 were higher than that of wild-type TNF (wtTNF), despite the loss of their TNFR2 affinities. TNFR1- and TNFR2-mediated bioactivities were assessed by HEp-2 and PC60-hTNFR2 assays, respectively. Interestingly, R1-selective candidates from Library I showed more potent activity via TNFR1 than those from Library II. R1-5 and R1-6 showed superior bioactivity and receptor selectivity. R1-6 was selected as the best overall mutant with greater than 1800-fold selective TNFR1 activity. These mutants were novel because TNFR1-selective mutants with higher bioactivity had not yet been established. Similar studies were performed with the TNFR2-selective candidates. In SPR analysis, these candidates showed higher TNFR2 affinity than wtTNF. Unfortunately, however, none of the TNFR2-selective candidates could sufficiently activate TNFR2 and had less than 40% of the bioactivity of wtTNF.

Next, we performed a competitive binding assay to confirm the details of the TNFR1 selectivity of R1-5 and R1-6—the candidates with the highest selectivity for TNFR1. Competitive affinities were assessed under a certain amount of wtTNF-FLAG, wtTNF fusing FLAG-tag (DYKDDDDK) at C-terminal, as competitor (Fig. 2). Similar to the results of the SPR analysis, R1-5 showed a higher affinity for TNFR1 compared with wild type, and its affinity for TNFR2 was decreased to approximately 10% that for wtTNF, suggesting that R1-5 was a TNFR1-selective mutant. In contrast to the SPR results, however, R1-6 showed a higher competitive affinity for TNFR1, and wtTNF–FLAG binding to TNFR2 was not completely inhibited, even by excess R1-6, which suggested that R1-6

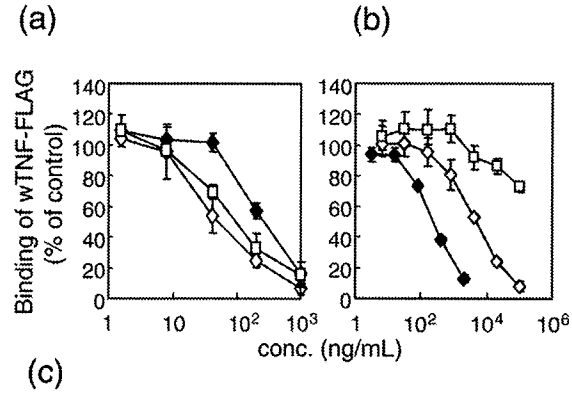

(c)

	TNFR1		TNFR2	
	IC50 (ng/ml)	(%)	IC50 (ngml)	(%)
wtTNF	276.0	100.0	508.1	100.0
R1-5	57.7	478.3	4606.6	11.0
R1-6	105.4	261.9	>100000.0	<0.5

Fig. 2. Competitive binding affinities of TNFR1-selective mutants (R1-5 and R1-6). Competitive affinities were assessed under 50 ng/ml FLAG-tagged wtTNF (wtTNF–FLAG) as competitor. Both (a) TNFR1 and (b) TNFR2 were immobilized. Binding of wtTNF–FLAG was inhibited by serially diluted TNF mutants. Final binding of wtTNF–FLAG was assessed by ELISA. Each value represents the mean±SD. (c) IC_{50} values are given as the concentration of the TNF mutant required to inhibit 50% of the maximal binding of wtTNF–FLAG.

lacked binding potency to TNFR2. Because the TNF binding interfaces to the receptors are known to overlap,[19] TNFR1 selectivity caused by a structural change in the R1-6 surface might provide important information for structure-based drug discovery.

X-ray crystallography of TNFR1-selective TNF mutant R1-6

The structural basis of the TNFR1 selectivity of R1-6 was examined by X-ray crystallography. After establishing crystallization conditions, good-quality crystals of R1-6 were obtained (approximately 0.2 mm×0.2 mm×0.3 mm in size). X-ray diffraction data were collected in SPring-8 (a large synchrotron radiation facility in Harima, Japan). Analysis of these data indicated that the space group is *R*3 and that the lattice constants are $a=135.87$ Å, $b=135.87$ Å, and $c=58.02$ Å (Table 3). The R1-6 structure was further refined using the CNS software suite. The results of model validation using the PROCHECK program indicated that there were 86.9% residues in the most favored regions, 13.1% residues in the additionally allowed regions, 0.0% residues in the generously allowed regions, and 0.0% residues in the disallowed regions.

The overall structures of the R1-6 [Protein Data Bank (PDB) code 2ZJC] and wtTNF (PDB code 1TNF) trimers are also similar and superimpose with an rmsd of 1.21 Å for 428 C^{α} atoms (Fig. 3). The structure of

Table 3. Crystallographic parameters and refinement statistics of the R1-6 crystal

Data collection	
Resolution (Å)	50–2.50 (2.59–2.50)
Cell constants (Å)[a]	135.9, 135.9, 58.0
Space group	*R*3
Measured reflections	74,516
Unique reflections	13,445 (1173)
Completeness (%)	99.9 (85.2)
R_{merge} (%)[b]	0.10 (0.53)
$I/\sigma(I)$	28.9 (4.2)
Refinement statistics	
Resolution (Å)	25.67–2.50
Reflections used	12,060
R_{cryst} (%)[c]	20.1
R_{free} (%)[d]	27.2
Completeness (%)	97.1
Atoms	
Protein; water	3338; 59
rmsd from ideality	
Bond lengths (Å); bond angles (°)	0.009; 1.27
Overall *B*-factor (Å^2)	19.7
B-factor rmsd (Å^2)	
Main-chain bonds; side-chain bonds	0.42; 0.77
Main-chain angles; side-chain angles	0.94; 1.48
Ramachandran plot statistics	
Most favored regions (%)	86.9
Additionally allowed regions (%)	13.1
Generously allowed regions (%)	0.0
Disallowed regions (%)	0.0

Values in parentheses are those for the outer shell.

[a] Cell constants are *a*, *b*, and *c*.

[b] $R_{merge} = \sum |I - \langle I \rangle| / \sum \langle I \rangle$, where I is intensity of the observations. R_{merge} in the last shell is high because of the anisotropic mosaicity of the crystal.

[c] $R_{cryst} = \sum ||F_o| - |F_c|| / \sum |F_o|$, where F_o and F_c are the observed and calculated structure factors, respectively.

[d] R_{free} is calculated as for R_{cryst}, but for the test set comprising reflections not used in refinement. The overall *B*-factor was calculated after TLS parameter analysis (TLSANL) using Refmac.

each monomer is similar to each other (rmsd of 0.98–1.12 Å for 140 C^α atoms). Especially, the structures of the β-sheet in each monomer are essentially the same (rmsd of 0.31–0.42 Å for 63 C^α atoms). These features have been found in the wtTNF trimer.[25]

The R1-6 loop structure near mutational residues 31 and 32 is different from that in wtTNF (Fig. 4). This loop structure between monomers is not different (wtTNF: rmsd of 0.61–0.72 Å for 11 C^α atoms; R1-6: rmsd of 0.39–0.91 Å for 11 C^α atoms) (Fig. 4a and b). However, they are clearly different between wtTNF and R1-6 (Fig. 4c). This structural change is thought to be caused by R32G mutation from a sterically bulky arginine residue to a flexible glycine residue. Because this region is close to the TNFR surface, such a structural change in the C^α chain could influence receptor binding. Additional TNF–TNFR docking simulation studies are discussed below.

Discussion

We recently developed the technology to create functional mutant proteins with high bioactivity, high *in vivo* stability, and antagonistic activity.[21–23] Here, we attempted to establish fully bioactive receptor-selective TNF mutants for functional analysis of TNFR1 and TNFR2 using our optimized phage display system. We constructed TNF mutant libraries (Libraries I and II) in which six residues near the receptor binding region were randomized (Fig. 1). From these libraries, we screened for TNFR1- or TNFR2-selective binders, and isolated receptor-selective candidates (Table 1). Despite the successful isolation of TNFR2-selective binders, the TNFR2-selective candidates obtained could not sufficiently activate TNFR2. This result suggested that the production of TNFR2-selective mutants was very rare in our library and that an improved panning method was necessary.

One advantage of our phage-display-based technique is that it can be used to obtain the sequence information of many mutants (Table 1). Tyr87 of TNF was conserved in all mutants obtained from Library II. This residue is highly conserved throughout the TNF superfamily, such as in LTα, LTβ, and LIGHT, and site-directed mutagenesis of the Tyr87 residue of TNF results in a dramatic loss of its biologic activity and its affinities for both TNFR1 and TNFR2.[17] In addition, Tyr87 replacement in antagonistic TNF causes unstable receptor binding and loss of receptor activation in our report.[23] These findings together indicate that Tyr87 is an essential residue for receptor signaling and receptor complex stability.

TNFR1-selective mutants had mutations near residue 30 and conserved residues near residue 140. In contrast, TNFR2-selective mutants had mutations near residue 140 and conserved residues near residue 30. These findings support those of previous point mutation analyses[15–17] and suggest that our phage-

Fig. 3. Overall structure of wtTNF and R1-6. Merge image of previously reported wtTNF structure (green; 1TNF) and refined structure of R1-6 (white; 2ZJC). The flexible loop containing residues 100–110 shown at the bottom of the figure was disordered in the R1-6 structure.

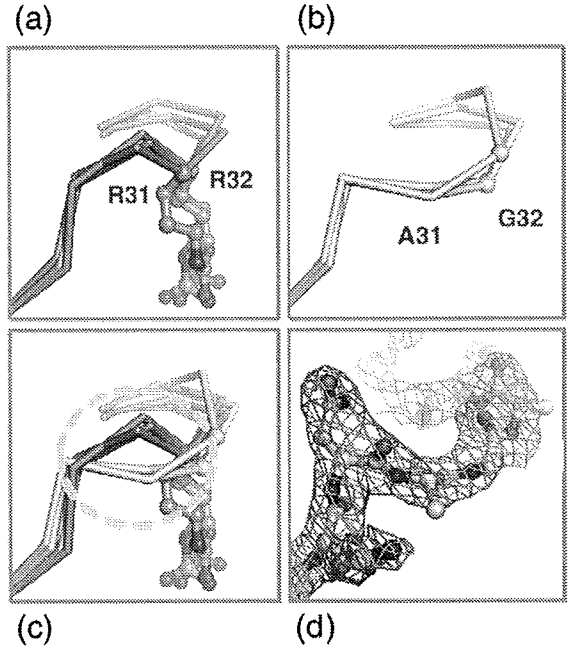

Fig. 4. Structural difference in receptor binding loop between wtTNF and R1-6. Each TNF monomer was superimposed using the CCP4i program. Details of the receptor binding loop, including residues 31 and 32, are shown in these figures. (a) Loops of wtTNF monomers (green); (b) loops of R1-6 monomers (white); (c) merged image of the loops of wtTNF and R1-6; (d) $2F_o-F_c$ map contoured at 1.0σ of R1-6 loop (pink mesh). The different C^α chains are highlighted by the dashed orange circle in (c).

display-based technique can be used to rapidly gather important information about the function–sequence relationships determined by long-term point mutation analysis. In the present study, we successfully isolated mutants that retained TNFR affinity from a huge phage library containing over a million repertoires. Most of the mutants in the library had no TNFR affinity and were therefore discarded through this selection step. This finding may indicate that the mutational residues in these unbound clones diminish TNFR affinity. This method may be useful for examining the function, capability, and sequence–function relationship of unknown cytokines and proteins.

Using these receptor-selective candidates, we expressed recombinant proteins and estimated their bioactivities and affinities for TNFR1 and TNFR2. R1-6, the most highly TNFR1-selective mutant, bound and activated TNFR1 efficiently despite the loss of its affinity for TNFR2. X-ray crystallography of R1-6 revealed that the crystal structure of R1-6 was a trimer (similar to wtTNF), and no other salient differences in the overall structure were observed. Superimposition of wtTNF and R1-6 sequences, however, revealed that the C^α of the receptor binding loop near residue 30 was partially different (Fig. 4). This change might influence the receptor binding mode of R1-6. We further used the superimposition program to perform docking simulations with TNF and TNFR1 based on the crystal structure of the LTα–TNFR1 complex (PDB code 1TNR).[18]

Based on the model wtTNF–TNFR1 complex, Arg31 of TNF would interact electrostatically with Glu56 of TNFR1. The main chain of TNF was too close to His69 of TNFR1, however, potentially causing potential steric hindrance (Fig. 5a). On the other hand, a structural change in the loop in R1-6, however, was thought to solve this problem (Fig. 5b). Arg32 of wtTNF associated with Ser72 of TNFR1 (Fig. 5a). In the R1-6 structure, however, this role of Arg32 was thought to be compensated for by Lys29 (Fig. 5b). This speculation was supported by the crystal structure of the LTα–TNFR1 complex.[18] The position of Lys29 in R1-6 corresponded to that of Arg46 in LTα interacting with Ser72 of TNFR1 by hydrogen bonding. This interesting "compensating role of an amino acid" would be difficult to induce using single point mutation methods, which is another advantage of our modified phage display technique.

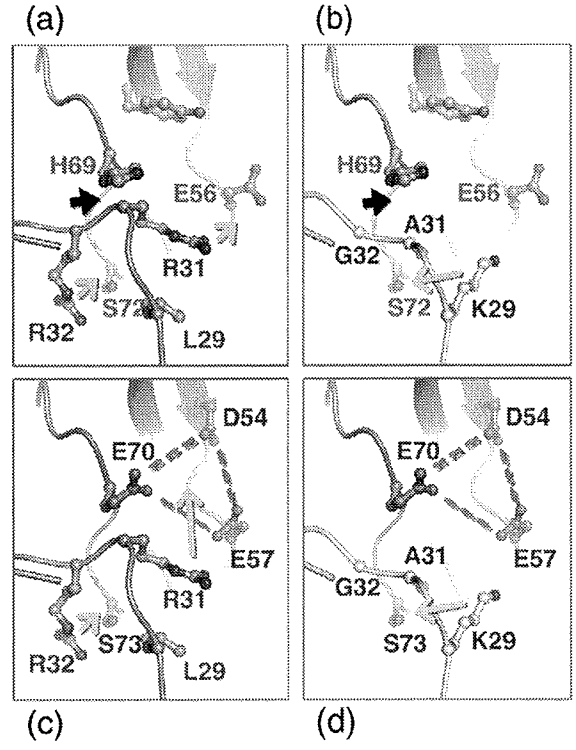

Fig. 5. Model of TNF binding to TNFR1 and TNFR2. Receptor binding interfaces of (a) wtTNF–TNFR1 (green–red); (b) R1-6–TNFR1 (white–red); (c) wtTNF–TNFR2 (green–blue); and (d) R1-6–TNFR2 (white–blue). The TNF–TNFR1 model complex was constructed from 1TNF (wtTNF) and 1TNR (LTα–TNFR1 complex). The predicted TNFR2 structure was constructed by side-chain mutation using the O program. In this simulation, the side chains of each structure were rotated to fit the predicted interaction. Stable structures of these rotamers were constructed using the O program. Steric hindrance might have occurred between His69 of TNFR1 and Arg32 of wtTNF in (a) (black arrowhead). Potential interactions are indicated by orange arrows. A cluster of anionic charged residues (Asp54, Glu57, and Glu70) is highlighted by a broken red line.

Next, we examined the TNFR1 selectivity of R1-6 based on its structure. Because the structure of TNFR2 is thought to be similar to that of TNFR1,[18] we generated a model structure of TNFR2 by manual mutation based on the crystal structure of TNFR1. This TNF–TNFR2 simulation is speculative, but this model, together with the information obtained from previous mutation studies, can be used to form hypotheses regarding the important structural features for TNFR1 selectivity. The binding surface of TNFR2 was composed of Asp54, Glu57, and Glu70, which could cause a strongly negatively charged surface of TNFR2 different from that of TNFR1 (Fig. 5c and d). Arg31 of wtTNF was thought to have an important role in TNFR2 binding by strongly interacting with this surface (Fig. 5c). R1-6 had an R31A mutation, however, which could cause the loss of the affinity of R1-6 for TNFR2 (Fig. 5d). In support of this finding, a single point mutation R31E mutant was previously reported to have a dramatic loss of affinity for TNFR2.[12,14] On the other hand, the R32W mutant is also reported to be a mutant with TNFR1 selectivity.[12] From our library, Arg32 of our TNFR1-selective candidates was replaced with hydrophobic or nonionic amino acids (Trp, Tyr, Phe, and Gly), which might indicate the importance of Arg32 for binding to TNFR2 (Table 1). This structural information, in combination with bioinformatics technology, will be useful for designing more advanced TNFR-selective mutants and TNFR-selective inhibitors (peptide mimics and chemical compounds).

In conclusion, the phage display technique is an attractive method for creating functional mutants, as demonstrated here by the production of TNFR-specific mutants. Application of this method to various cytokines and proteins will enhance the construction of useful receptor-selective mutants and accelerate functional analysis of these proteins. As an advanced application, analysis of the "structure (sequence)–function relationship" using the obtained mutants will be a powerful technique for basic life science research and drug discovery.

Materials and Methods

Cell culture

HEp-2 cells (a human fibroblast cell line) were provided by the Cell Resource Center for Biomedical Research (Tohoku University) and maintained with RPMI 1640 containing 10% fetal bovine serum and antibiotics. PC60-hTNFR2 cells (a mouse–rat fusion hybridoma comprised of human TNFR2-transfected PC60 cells) were provided by Dr. Vandenabeele and maintained in RPMI 1640 supplemented with 10% fetal bovine serum, 1 mM sodium pyruvate, 5×10^{-5} M 2-mercaptoethanol, 3 μg/ml puromycin, and antibiotics (100 U/ml penicillin, 100 μg/ml streptomycin, and 0.25 μg/ml amphotericin B).

Library construction

The pCANTAB phagemid vector (GE Healthcare Ltd., UK) encoding mutTNF-Lys(−) was used as template for PCR. This TNF was previously reported to be a fully active lysine-deficient TNF mutant.[22] Mutations were introduced in TNF at six amino acid codons (Library I: amino acid residues 29, 31, 32, and 145–147; Library II: amino acid residues 84–89) using a two-step PCR. Three primers, Oligos A, B, and C, were used for the construction of Library I. The first PCR was performed using Oligos A and B. The PCR conditions were 5 min at 95 °C, 35 cycles of denaturization at 95 °C for 15 s, and annealing/extension at 68 °C for 2 min. This first PCR product and Oligo C were then annealed to the template, and PCR was performed again under the same conditions. For the construction of Library II, Oligos A, D, and E were used. The first PCR was performed using Oligos A and D. The first PCR product and Oligo E were used as primers for the second PCR. The PCR conditions of Library II were the same as those of Library I. After the second PCR, the PCR products were digested with HindIII and NotI, and then ligated to a pY03′ phagemid vector (modified from pCANTAB) for the display of TNF variants on the phage surface as g3p fusion proteins. The primer sequences used in this experiment are listed below. Oligos A and E were designed to prime to the pCANTAB vector sequence: Oligo A: 5′-GATAACAATTTCACACAGGAAACAGCTATGACCATGATTACGCCAAGCTTTGGAGCC-3′; Oligo B: 5′-CGCCATTGGCCAGGAGGGCATTAGCSNNSNNGTTSNNCCACTGGAGCTGCCCCTCAGCTTGAGGG-3′; Oligo C: 5′-CCAGCGGATCCGGATACGGCACCGGCGCACCTGCGGCCGCGGATCCACCACCACCCAGGGCAATGATCCCAAAGTAGACCTGCCCSNNSNNSNNAAAGTCGAGATAGTCGGGCCGATTGA-3′; Oligo D: 5′-CTGGCAGGGGCTGCGGATGGCAGAGAGGAGATTGACGGGSNNSNNSNNSNNSNNGATGCGGCTGATGGTGTGGGTGAGGAGCAC-3′; Oligo E: 5′-TGCGGCACGCGGTTCCAGCGGATC-3′.

Isolation of receptor-selective TNF mutants from the library (affinity panning and screening)

Human TNFR1 Fc (R&D Systems, Inc., Minneapolis, MN) and TNFR2 Fc (R&D Systems, Inc.) were diluted to 50 μg/ml in 10 mM sodium acetate buffer (pH 4.5) and immobilized on a CM3 sensor chip using an amine coupling kit (GE Healthcare Ltd.), which resulted in an increase of 4000–6000 resonance units. The phage library (1×10^{11} colony-forming units/100 μl) was injected at 3 μl/min over the sensor chip. After binding and until the association phase had been reached, the sensor chip was washed using the rinse command and eluted using 20 μl of 10 mM glycine–HCl. The eluted phage was neutralized with 1 M Tris–HCl (pH 6.9). *E. coli* (TG1) was infected with the collected phage for amplification. This panning cycle was performed two more times. After picking up a single clone of transfected *E. coli*, the phagemid vectors were sequenced using a Big Dye Terminator v3.1 kit and ABI PRISM 3100 (Applied Biosystems Ltd., Pleasanton, CA). After the procedure, the binding affinities of the TNF mutants were assessed by ELISA, and their bioactivities through TNFR1 were determined by cytotoxicity assay in human HEp-2 cells.

Expression and purification of TNF mutants

The protocol for the expression and purification of recombinant protein was the same as that described previously.[21,22] Briefly, TNF mutants were produced in the *E. coli* BL21(DE3) strain. The inclusion body of each

TNF mutant was washed in 2.5% Triton X-100 and solubilized in 6 M guanidine–HCl, 0.1 M Tris–HCl (pH 8.0), and 2 mM ethylenediaminetetraacetic acid. Solubilized protein at 10 mg/ml was reduced with 10 mg/ml dithioerythritol for 4 h at room temperature and refolded by 100-fold dilution in a refolding buffer (100 mM Tris–HCl, 2 mM ethylenediaminetetraacetic acid, 0.5 M arginine, and 551 mg/L oxidized glutathione). After dialysis with 20 mM Tris–HCl (pH 7.4) containing 100 mM urea, active trimeric proteins were purified by ion-exchange chromatography using Q-Sepharose FF (GE Healthcare Ltd.). Size-exclusion chromatography was performed using a Superose 12 column (GE Healthcare Ltd.).

In vitro bioactivity of TNF mutants

HEp-2 cells were used for cytotoxicity assay in the presence of cycloheximide (50 μg/ml). HEp-2 cytotoxicity was dependent on TNFR1 signaling. HEp-2 cells were cultured in 96-well plates in the presence of TNF mutants and serially diluted mouse or human wtTNF (PeproTech EC Ltd., UK) at 4×10^4 cells/well. For neutralization assay, cells were cultured in the presence of a constant concentration of human (20 ng/ml) wtTNF and a serial dilution of TNF mutants. After incubation for 18 h, cell survival was determined by methylene blue assay, as described previously.[21,22] To evaluate the bioactivity of the TNF mutant binding specifically to TNFR2, PC60-hTNFR2 cells were used as an index of granulocyte–macrophage colony-stimulating factor (GM-CSF) production, as described previously.[26] Briefly, PC60-hTNFR2 cells were cultured at 5×10^4 cells/well with interleukin-1β (2 ng/ml) and serially diluted TNF mutant. After 24 h of incubation, the amount of rat GM-CSF produced was quantified by ELISA in accordance with the manufacturer's protocol (R&D Systems, Inc.).

Affinity assessment using SPR

The binding kinetics of wtTNF and TNF mutants were analyzed using the BIAcore 3000 SPR system (GE Healthcare Ltd.). TNFRs were immobilized on a CM5 sensor chip, which resulted in an increase of 3000–5000 resonance units. During the association phase, TNF mutants or wtTNF diluted in HBS-EP running buffer (10 mM HEPES pH7.4, 150 mM NaCl, 3 mM EDTA, 0.005% Tween20, GE Healthcare Ltd.) at 78.4, 26.1, or 8.7 nM were individually passed over the immobilized TNFR at a flow rate of 20 μl/min. During the dissociation phase, HBS-EP buffer was applied to the sensor chip at a flow rate of 20 μl/min. The data were analyzed globally with BIAEVALUATION 3.0 software (GE Healthcare Ltd.) using a 1:1 binding model.

Competitive binding of TNF to TNFR1 and TNFR2 (ELISA)

Goat anti-human IgG (MP Biomedicals, Inc., Solon, OH) was immobilized on Maxisorb 96-well ELISA plates (Nalge Nunc International KK, Japan), and nonspecific binding to the plates was blocked using Block Ace (Dainippon Sumitomo Pharma Co., Ltd., Japan). Human TNFR1-Fc or human TNFR2-Fc (ALEXIS Corporation, Switzerland) was bound to coated antibody. Serially diluted TNF with 50 ng/ml FLAG-tagged wtTNF (wtTNF–FLAG) was added to TNFR1-Fc or TNFR2-Fc in 0.4% Block Ace. wtTNF–FLAG binding was detected by anti-FLAG M2 antibody (Sigma-Aldrich Corporation, St. Louis, MO) and avidin horseradish peroxidase conjugate (Invitrogen Corporation, Carlsbad, CA). The binding affinity of TNF was assessed by competitive wtTNF–FLAG binding to TNFR (IC_{50} value).

X-ray crystallography

Purified R1-6 was concentrated to 10 mg/ml in 20 mM Tris–HCl (pH 7.4). Initial screening using a Hampton Crystal screen 1-2 and Crystal screen Lite kit (Hampton Research Corporation, Aliso Viejo, CA) was performed by vapor diffusion method with hanging drops (1 + 1 μl) at 20 °C. After optimization of the crystallization conditions, rhombohedral crystals (0.2 mm × 0.2 mm × 0.3 mm) were obtained with reservoir solution containing 0.5 M ammonium sulfate, 1.2 M lithium sulfate, and 0.1 M trisodium citrate (pH 5.6). The crystals were frozen in a cryopreserving solution containing 15% glycerol as cryoprotectant. X-ray diffraction data to 2.5 Å resolution were collected at BL41XU, SPring-8, under flash cooling to 100 K to reduce the effects of radiation damage. Data integration and scaling were performed using HKL2000.[27] Molecular replacement was performed by the MOLREP program in CCP4i[28] using a crystal structure of the wtTNF (1TNF)[25] as search model. Cycles of manual rebuilding using the O program[29] and refinement using the CNS program[30] led to a refined structure. Final refinement (TLS refinement) was performed using the Refmac program in CCP4i.[28] Final model validation was performed using PROCHECK program in CCP4i.[28] The model complexes of TNF–TNFR1 and R1-6–TNFR1 were constructed based on the crystal structure of the LTα–TNFR1 complex[18] using the superimposing program in CCP4i. Structural models of TNFR2 were constructed based on the TNFR1 structure by manual mutation using the O program.[29]

Accession number

Coordinates and structure factors have been deposited in the PDB with accession number 2ZJC.

Acknowledgements

This study was supported by Research for Promoting Technological Seeds (no. 11-067) from the Japan Science and Technology Agency; Research Fund Project on Health Sciences focusing on Drug Innovation (no. KAA3701) from the Japan Health Sciences Foundation; the Global COE Program "*In Silico* Medicine" (Wakate-16) at Osaka University; a Grant-in-Aid for Young Scientists (B) (no. 20790134) and Grants-in-Aid for Scientific Research (nos. 18015055 and 17689008) from the Ministry of Education, Culture, Sports, Science, and Technology of Japan; and Research Fellowships for Young Scientists (no. 20-3919) from the Japan Society for the Promotion of Science.

References

1. Aggarwal, B. B. (2003). Signalling pathways of the TNF superfamily: a double-edged sword. *Nat. Rev. Immunol.* **3**, 745–756.

2. Feldmann, M. & Maini, R. N. (2003). Lasker Clinical Medical Research Award. TNF defined as a therapeutic target for rheumatoid arthritis and other autoimmune diseases. *Nat. Med.* **9**, 1245–1250.
3. Kooloos, W. M., de Jong, D. J., Huizinga, T. W. & Guchelaar, H. J. (2007). Potential role of pharmacogenetics in anti-TNF treatment of rheumatoid arthritis and Crohn's disease. *Drug Discov. Today*, **12**, 125–131.
4. Rutgeerts, P., Van Assche, G. & Vermeire, S. (2004). Optimizing anti-TNF treatment in inflammatory bowel disease. *Gastroenterology*, **126**, 1593–1610.
5. Rothe, J., Lesslauer, W., Lötscher, H., Lang, Y., Koebel, P., Köntgen, F. *et al.* (1993). Mice lacking the tumour necrosis factor receptor 1 are resistant to TNF-mediated toxicity but highly susceptible to infection by *Listeria monocytogenes*. *Nature*, **364**, 798–802.
6. Kafrouni, M. I., Brown, G. R. & Thiele, D. L. (2003). The role of TNF–TNFR2 interactions in generation of CTL responses and clearance of hepatic adenovirus infection. *J. Leukocyte Biol.* **74**, 564–571.
7. Rahman, M. M. & McFadden, G. (2006). Modulation of tumor necrosis factor by microbial pathogens. *PLoS Pathog.* **2**, e4.
8. Chan, F. K., Shisler, J., Bixby, J. G., Felices, M., Zheng, L., Appel, M. *et al.* (2003). A role for tumor necrosis factor receptor-2 and receptor-interacting protein in programmed necrosis and antiviral responses. *J. Biol. Chem.* **278**, 51613–51621.
9. Wajant, H., Pfizenmaier, K. & Scheurich, P. (2003). Tumor necrosis factor signaling. *Cell Death Differ.* **10**, 45–65.
10. Weiss, T., Grell, M., Siemienski, K., Mühlenbeck, F., Dürkop, H., Pfizenmaier, K. *et al.* (1998). TNFR80-dependent enhancement of TNFR60-induced cell death is mediated by TNFR-associated factor 2 and is specific for TNFR60. *J. Immunol.* **161**, 3136–3142.
11. Fotin-Mleczek, M., Henkler, F., Samel, D., Reichwein, M., Hausser, A., Parmryd, I. *et al.* (2002). Apoptotic crosstalk of TNF receptors: TNF-R2-induces depletion of TRAF2 and IAP proteins and accelerates TNF-R1-dependent activation of caspase-8. *J. Cell Sci.* **115**, 2757–2770.
12. Van Ostade, X., Vandenabeele, P., Everaerdt, B., Loetscher, H., Gentz, R., Brockhaus, M. *et al.* (1993). Human TNF mutants with selective activity on the p55 receptor. *Nature*, **361**, 266–269.
13. Barbara, J. A., Smith, W. B., Gamble, J. R., Van Ostade, X., Vandenabeele, P., Tavernier, J. *et al.* (1994). Dissociation of TNF-alpha cytotoxic and pro-inflammatory activities by p55 receptor- and p75 receptor-selective TNF-alpha mutants. *EMBO J.* **13**, 843–850.
14. Van Ostade, X., Vandenabeele, P., Tavernier, J. & Fiers, W. (1994). Human tumor necrosis factor mutants with preferential binding to and activity on either the R55 or R75 receptor. *Eur. J. Biochem.* **220**, 771–779.
15. Van Ostade, X., Tavernier, J. & Fiers, W. (1994). Structure–activity studies of human tumour necrosis factors. *Protein Eng.* **7**, 5–22.
16. Yamagishi, J., Kawashima, H., Matsuo, N., Ohue, M., Yamayoshi, M., Fukui, T. *et al.* (1990). Mutational analysis of structure–activity relationships in human tumor necrosis factor-alpha. *Protein Eng.* **3**, 713–719.
17. Zhang, X. M., Weber, I. & Chen, M. J. (1992). Site-directed mutational analysis of human tumor necrosis factor-alpha receptor binding site and structure–functional relationship. *J. Biol. Chem.* **267**, 24069–24075.
18. Banner, D. W., D'Arcy, A., Janes, W., Gentz, R., Schoenfeld, H. J., Broger, C. *et al.* (1993). Crystal structure of the soluble human 55 kD TNF receptor-human TNF beta complex: implications for TNF receptor activation. *Cell*, **73**, 431–445.
19. Fu, Z. Q., Harrison, R. W., Reed, C., Wu, J., Xue, Y. N., Chen, M. J. & Weber, I. T. (1995). Model complexes of tumor necrosis factor-alpha with receptors R1 and R2. *Protein Eng.* **8**, 1233–1241.
20. Reed, C., Fu, Z. Q., Wu, J., Xue, Y. N., Harrison, R. W., Chen, M. J. & Weber, I. T. (1997). Crystal structure of TNF-alpha mutant R31D with greater affinity for receptor R1 compared with R2. *Protein Eng.* **10**, 1101–1107.
21. Shibata, H., Yoshioka, Y., Ikemizu, S., Kobayashi, K., Yamamoto, Y., Mukai, Y. *et al.* (2004). Functionalization of tumor necrosis factor-alpha using phage display technique and PEGylation improves its anti-tumor therapeutic window. *Clin. Cancer Res.* **10**, 8293–8300.
22. Yamamoto, Y., Tsutsumi, Y., Yoshioka, Y., Nishibata, T., Kobayashi, K., Okamoto, T. *et al.* (2003). Site-specific PEGylation of a lysine-deficient TNF-alpha with full bioactivity. *Nat. Biotechnol.* **21**, 546–552.
23. Shibata, H., Yoshioka, Y., Ohkawa, A., Minowa, K., Mukai, Y., Abe, Y. *et al.* (2008). Creation and X-ray structure analysis of the tumor necrosis factor receptor-1-selective mutant of a tumor necrosis factor-alpha antagonist. *J. Biol. Chem.* **283**, 998–1007.
24. Loetscher, H., Stueber, D., Banner, D., Mackay, F. & Lesslauer, W. (1993). Human tumor necrosis factor alpha (TNF alpha) mutants with exclusive specificity for the 55-kDa or 75-kDa TNF receptors. *J. Biol. Chem.* **268**, 26350–26357.
25. Eck, M. J. & Sprang, S. R. (1989). The structure of tumor necrosis factor-alpha at 2.6 A resolution. Implications for receptor binding. *J. Biol. Chem.* **264**, 17595–17605.
26. Abe, Y., Yoshikawa, T., Kamada, H., Shibata, H., Nomura, T., Minowa, K. *et al.* (2008). Simple and highly sensitive assay system for TNFR2-mediated soluble- and transmembrane-TNF activity. *J. Immunol. Methods*, **335**, 71–78.
27. Otwinowski, Z. & Minor, W. (1997). Processing of X-ray diffraction data collected in oscillation mode. *Methods Enzymol.* **276**, 307–326.
28. Potterton, E., Briggs, P., Turkenburg, M. & Dodson, E. (2003). A graphical user interface to the CCP4 program suite. *Acta Crystallogr. Sect. D*, **59**, 1131–1137.
29. Jones, T. A., Zou, J. Y., Cowan, S. W. & Kjeldgaard, M. (1991). Improved methods for building protein models in electron density maps and the location of errors in these models. *Acta Crystallogr. Sect. A*, **47** (Pt 2), 110–119.
30. Brunger, A. T., Adams, P. D., Clore, G. M., DeLano, W. L., Gros, P., Grosse-Kunstleve, R. W. *et al.* (1998). Crystallography and NMR system: a new software suite for macromolecular structure determination. *Acta Crystallogr. Sect. D*, **54**, 905–921.